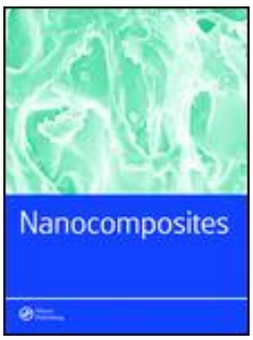

Nanocomposites

ISSN: 2055-0324 (Print) 2055-0332 (Online) Journal homepage: http://www.tandfonline.com/loi/ynan20

Bioactive nanocomposites for dental application obtained by reactive suspension method

Oussama Boumezgane, Federica Bondioli, Sergio Bortolini, Alfredo Natali, Aldo R. Boccaccini, Elena Boccardi & Massimo Messori

To cite this article: Oussama Boumezgane, Federica Bondioli, Sergio Bortolini, Alfredo Natali, Aldo R. Boccaccini, Elena Boccardi & Massimo Messori (2016) Bioactive nanocomposites for dental application obtained by reactive suspension method, Nanocomposites, 2:1, 37-49, DOI: 10.1080/20550324.2016.1187447

To link to this article: http://dx.doi.org/10.1080/20550324.2016.1187447

Published online: 01 Jul 2016.

Nanocomposites Original Research Paper

Bioactive nanocomposites for dental application obtained by reactive suspension method

Oussama Boumezgane[1,2], Federica Bondioli[3], Sergio Bortolini[4], Alfredo Natali[4], Aldo R. Boccaccini[5], Elena Boccardi[5] and Massimo Messori[1,2]*

[1]Dipartimento di Ingegneria "Enzo Ferrari", Università di Modena e Reggio Emilia, via P. Vivarelli 10/1, Modena, Italy
[2]Consorzio INSTM, Unità di ricerca di Modena e Reggio Emilia, via Giusti 9, Firenze, Italy
[3]Dipartimento di Ingegneria Industriale, Università di Parma, Parco Area delle Scienze 181/A, Parma, Italy
[4]Dipartimento Chirurgico, Medico, Odontoiatrico e di Scienze Morfologiche con Interesse Trapiantologico, Oncologico e di Medicina Rigenerativa, Università di Modena e Reggio Emilia, via del Pozzo 71, Modena, Italy
[5]Department of Materials Science and Engineering, University of Erlangen-Nuremberg,Cauerstraße 6, Erlangen, Germany

Abstract Hydroxyapatite (HA) filled poly(methyl methacrylate)/poly(hydroxyethyl methacrylate) (PMMA/PHEMA) blends were prepared by reactive suspension method: HA was synthesized by co-precipitation process directly within a HEMA solution and the so-obtained suspension was polymerized in the presence of PMMA. HA particles were obtained in form of nanorods with a length of 50–200 nm and a diameter of 10–30 nm. A significant increase in glass transition temperature was observed in the nanocomposites with respect to the unfilled polymer blends. Dynamic-mechanical thermal analysis showed a significant increase in the storage modulus in the nanocomposites measured in the rubbery region. This increase was unpredicted by Mooney's predictive equation and was attributed to the presence of cross-linking points due to the *in situ* generated HA particles. An increase in the elastic modulus was also observed at room temperature in compression and three-point bending tests. The presence of HA in the polymer blends resulted in an important decrease in the water sorption values. The bioactivity of the nanocomposites was verified by the precipitation of HA layer on the surface after soaking in simulated body fluid.

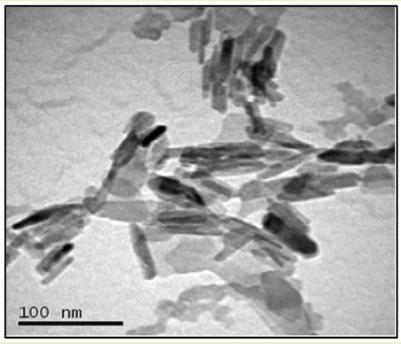

Reactive suspension method: synthesis of hydroxyapatite within hydroxyethyl methacrylate as suspending medium and polymerizable monomer.

Hydroxyapatite nanoparticles of acicular shape (length 50-200 nm and diameter 10-30 nm, average aspect ratio of 6).

Keywords Nanocomposites, Nanoparticles, Polymer-matrix composites, Bioactivity, Hydroxyapatite

Cite this article Oussama Boumezgane, Federica Bondioli, Sergio Bortolini, Alfredo Natali, Aldo R. Boccaccini, Elena Boccardi and Massimo Messori: *Nanocomposites*, 2016, 1, 37–49.

Introduction

Oral health has become increasingly important during the last decades. In this respect, dental restorative materials have received particular attention by numerous researchers, especially in the area of extensively used acrylic-based – resins. A large number of investigations have been performed to improve the properties of composite resins for dental applications, such as abrasion resistance, mechanical, and anti-bacterial properties.[1,2]

Acrylic materials, consist of a solid component (poly (methyl methacrylate) powder, PMMA) and a liquid component (methyl methacrylate monomer), are one of the most frequently and extensively used dental restorative materials, due to their satisfactory aesthetic properties, easy operation, low cost, and good stability in the oral environment.[2] The most common use of this material includes the fabrication of denture base, temporary crowns, and temporal seal of cavities.[3]

One method of improving the mechanical properties of an acrylic-based denture base is by adding preformed nanoparticles (*ex situ* approach) into the liquid phase before mixing with

*Corresponding author, email massimo.messori@unimore.it

Received 22 January 2016; accepted 3 May 2016
DOI 10.1080/20550324.2016.1187447

the PMMA powders. The most common nanoparticle fillers used are silica, zirconia, titania, alumina, and hydroxyapatite.[4–6] The use of nanoparticles can improve the resin properties such as wear resistance, modulus, and flexural strength even at very low mass fraction values. However, these properties are greatly influenced by the quality of the nanofiller dispersion in the polymeric matrix. Because of the very high surface area and surface charge of inorganic nanoparticles, agglomerates are generally formed, and thus the homogeneous dispersion of nanofillers in the organic matrix becomes difficult at high filler concentration. In fact, particles, with a size less than 100 nm, tend to agglomerate into larger clusters to minimize their surface energy. This agglomeration affects materials performance by the inclusion of voids that act as preferential sites for crack initiation and failure.[7]

A common method to limit agglomeration phenomena is the chemical modification of particles using suitable coupling agents, which decrease the surface energy of the particles and improve the compatibility with the organic matrix. The main drawback of this approach is the time-consuming steps of chemical modification and purification of particles. An alternative approach is represented by the synthesis of the nanoparticles directly within the organic matrix (*in situ* approach).

In this respect, the aim of this study is to realize an innovative nanocomposite material using PMMA in form of powder and hydroxyethyl methacrylate (HEMA) as liquid phase, reinforced with *in situ* generated hydroxyapatite ($Ca_{10}(PO_4)_6(OH)_2$, HA) nanoparticles. HA is an osteogenic and osteoconductive inorganic phase,[8] similar to the bone mineral, and confers its bioactivity to polymer-based composites promoting bone regeneration.[9–15]

In the present work, the so-called 'reactive suspension method'[16] is used. The *in situ* synthesis in a HEMA solution of HA by a co-precipitation process, starting from calcium nitrate tetrahydrate and ammonium dihydrogen phosphate as precursors, is proposed as a promising strategy for the achievement of homogeneous hybrid materials having higher degree of phase interaction between the polymer matrix and the inorganic filler. This procedure should avoid extensive particles agglomeration typically seen in polymer/HA composites obtained by mechanical incorporation of preformed HA powders into the polymer melt or solution, causing non-homogeneous materials, and it was already proved to be an effective approach for the preparation of homogeneous PCL/silicate glasses composites,[17,18] poly(propylene fumarate)/HA composites,[19] PCL/HA composites,[16] and polyacrylic acid/calcium phosphate ceramics composites.[20]

In this study, the structure and morphology of the obtained PMMA/HEMA/HA composites are investigated. The mechanical properties are determined in flexural and compression mode, while the bioactivity of the composites is studied by immersion in simulated body fluid (SBF).

Materials and methods

Materials

Calcium nitrate tetrahydrate ($Ca(NO_3)_2{\cdot}4H_2O$), HEMA, 3-(trimethoxysilyl)propyl methacrylate (MSDS), and dibenzoyl peroxide (BPO) were purchased from Sigma–Aldrich (Milan, Italy). Ammonium phosphate ($(NH_4)_2HPO_4$), ammonium hydroxide (NH_4OH), and ethanol were purchased from Carlo Erba (Italy). PMMA powder was obtained from Lang Dental Manufacturing Co. under the trade name of Jet Kit. Reagent-grade NaCl, $NaHCO_3$, KCl, $K_2HPO_4{\cdot}3H_2O$, $MgCl_2{\cdot}6H_2O$, Na_2SO_4, 1 M HCl, and Tris buffer ($(CH_2OH)_3CNH_2$), used for SBF preparation, were purchased from Sigma–Aldrich.

Synthesis of hydroxyapatite, $Ca_{10}(PO_4)_6(OH)_2$

The reagents used to synthesize HA were $Ca(NO_3)_2{\cdot}H_2O$ and $(NH_4)_2HPO_4$[21] (Table 1). $Ca(NO_3)_2{\cdot}H_2O$ was dissolved in HEMA to obtain a 0.259 M solution and $(NH_4)_2HPO_4$ was dissolved in distilled water to obtain a 0.156 M aqueous solution. 50 mL of $(NH_4)_2HPO_4$ aqueous solution was added drop wise into 50 mL of $Ca(NO_3)_2$/HEMA solution under vigorous stirring at 65 °C over a period of approximately 1 h. Vigorous stirring was maintained for 1 h and the pH was periodically monitored and leveled at value 9 by addition of NH_4OH.

0.025 mmol of silane coupling agent MSDS[22] per m^2 of HA surface (see the evaluation of specific surface area of synthesized particles in Table 1) were then added to stabilize the suspension, avoiding the precipitation of HA nanoparticles, and increasing the compatibility between the organic phase (HEMA) and the inorganic nanoparticles.

To characterize the HA powder, the suspension was filtrated and the powder was washed with ethanol by centrifugation to solubilize and remove the organic solvent. After the drying step, the powder was accurately weighed in order to verify the reaction yield that is 100% (Table 1).

Nanocomposites preparation

PMMA powder was added to the HEMA/HA suspension in two different weight ratios, 1:2 and 1:3, respectively, under vigorous stirring, after the addition of 1 phr of BPO as radical initiator. The obtained nanocomposites formulations are listed in Table 2. Unfilled HEMA/PMMA samples were also prepared in the absence of HA, as reference materials.

The mixtures were then polymerized by thermal curing at 60 °C for 1 h with a post-curing at 100 °C for 1 h.

Powder and composites characterization

The structural characterization of the dried powders was performed by X-rays diffraction analysis (XRD) using an X'Pert PRO diffractometer (PANalytical), operating in the 10–90 2theta range with step size 0.01 ° and step time of 1 s.

Table 1 Composition of the synthesized powder and specific surface area (SSA) value (HA content expressed in parts per hundred of resin, phr)

Code	$Ca(NO_3)_2{\cdot}H_2O$ (g)	$(NH_4)_2HPO_4$ (g)	Theoretical HA (g)	Obtained HA (g)	HEMA (g)	HA content in HEMA (phr)	SSA (m^2/g)
HA	12.22	4.12	5.20	5.47	50.00	10.94	117.02

Table 2 Composition of the prepared samples

Code	PMMA/HEMA weight ratio	HA in PMMA-HEMA matrix (phr)
1:2 HA	0.5	7
1:3 HA	0.33	8

The particle morphology was examined by transmission electron microscopy (TEM, JEM 2010, Jeol, Japan). Dried powders were dispersed in *n*-butanol and a drop of the so-obtained suspension was placed on a copper grid (200 mesh) covered with PELCO® support films of Formvar (thickness of 30–60 nm), followed by drying.

To determine the amount of the silane coupling agent added to the HA suspension, the specific surface area of the powder was measured by the Brunauer, Emmett, and Teller method (Gemini 2360 apparatus, Micromeritics, Norcross, GA, USA) after degassing under vacuum at 150 °C.

In order to investigate the presence of residual organic groups on the particle surface, FT-IR analysis was performed on the obtained powder. The analysis was carried out in the attenuated total reflectance mode (ATR) with an Avatar 330 spectrometer (Thermo Nicolet, Germany). A minimum of 64 scans with a resolution of 1 cm^{-1} was performed.

Finally, simultaneous thermogravimetry and differential thermal analysis (TG-DTA) was performed, on the modified HA powder, with a Netzsch STA 429 CD with a heating rate of 20 °C·min^{-1} up to 1000 °C in air atmosphere.

The nanocomposites were characterized by differential scanning calorimetry (DSC) to measure the glass transition temperature (T_g) of composites and, analyzing the effect of the HA nanofiller on the glass transition temperature of composites. The test was carried out using a scanning rate of 25 °C min^{-1} from 0 to 200 °C and the T_g value was assumed as the mean value of the energy jump of the thermograms (average value between the onset and the endpoint of the glass-transition range).

Dynamic-mechanical thermal analysis (DMTA) was carried out on DMA Q800 TA instrument in the temperature range between −30 and +150 °C with a heating rate of 3 °C min^{-1} using a single cantilever clamp. The storage modulus E′ and tanδ were measured and the T_g value was assumed as the maximum of the tanδ curve.

Three-point bending test and compression test were performed using an Instron series 5500 dynamometer for flexural and compression tests on the sample with the highest content of HA (1:3 HA) and on the corresponding unfilled 1:3 sample.

Three-point bending test was carried out following the ISO 4049 standard procedure[23] for the flexural strength test. Five prismatic samples with 25 × 2 × 2 mm^3 were prepared. The samples were stored in water at 37 °C for 24 h just before the measurement. A crosshead speed of 0.75 mm·min^{-1} was applied until sample fracture.

Compression test was performed following the ISO 604 standard.[24] Five prismatic samples 10 × 10 × 4 mm^3 were prepared for both 1:3 HA sample and unfilled 1:3 sample. The samples were stored in water at 37 °C on the day before the measurement. A crosshead speed of 2 mm·min^{-1} was applied until sample fracture.

For water sorption test, the samples were cut in small pieces with prismatic shape, and then were placed in a desiccator at 37 °C until constant mass (m_1) was reached. The dried samples were stored in water at 37 °C for 7 days and weighted to get the wet mass (m_2) and then placed in a desiccator until a dried constant mass was reached (m_3).

The water sorption value was calculated by the formula:

$$W_{sp} = \frac{(m_2 - m_3)}{V} \quad (1)$$

where W_{sp} is the water sorption value in μg·mm^{-3} and V the sample volume.[23]

In vitro tests were carried out to assess the bioactivity of the nanocomposites. The SBF is an aqueous solution with inorganic ion composition very similar to human blood plasma; it is a protein-free solution with a pH of 7.4 prepared in the laboratory according to the procedure developed by Kokubo and Takadama,[25] and utilized by many other authors.[26–28] Proper quantities of the reagents NaCl, $NaHCO_3$, KCl, $K_2HPO_4 \cdot 3H_2O$, $MgCl_2 \cdot 6H_2O$, $CaCl_2$, Na_2SO_4, tris(hydroxymethyl) aminomethane, were dissolved in deionized water and the solution was buffered at pH7.4 at 36.5 °C by adding tris and 1 M HCl, with the help of a magnetic stirrer, according to the concentrations given in;[29] then, the pH of the solution was adjusted to 7.4 by addition of 1 M hydrochloric acid. The samples were cut in rectangular shape and immersed into SBF solution with a ratio SBF/material of 255 ml/g[26] maintained at body temperature (37 °C) in a rotating incubator. The samples were tested for four different periods of 1 h, 24 h, 7 days, and 28 days; in the case of 7 and 28 days, the SBF solution was changed every 3–4 days in order to better mimic *in vitro* the *in vivo* behavior of the material.[30] The samples were removed from SBF solution at the end of each treatment period, washed with deionized water and dried at room temperature.

To analyze the ability to form an apatite layer, the surface of the samples after SBF immersion was observed with an electron scanning microscopy (SEM) equipped with an energy-dispersive X-ray spectroscopy (EDS) using electron and ion beam microscope Zeiss Auriga 60. Infrared spectroscopy analysis was also carried out in ATR using an FT-IR machine (Nicolet 6700, Thermo Scientific Germany). The analysis was performed under the following conditions: spectral range between 4000 and 530 cm^{-1}; window material, CsI; 32 scans at a resolution of 4 cm^{-1}. Finally, X-ray diffraction (XRD) using an X'Pert PRO diffractometer (PANalytical), operating in the 10–90 2theta range with step size 0.01 ° and step time of 1 s, was carried out to determine the phase composition of the crystallization on the surface of the samples.

Results and discussion

HA nanoparticles characterization

Figure 1 reports the XRD pattern of the HA powder obtained with Ca/P in 1.67 stoichiometric ratio, such as that of HA present in natural bone tissues. The peaks in the XRD pattern were those characteristics of pure HA and closely matched with the JCPDS 09-432 of stoichiometric calcium hydroxyapatite, indicating the absence of other calcium phosphate phases.[31]

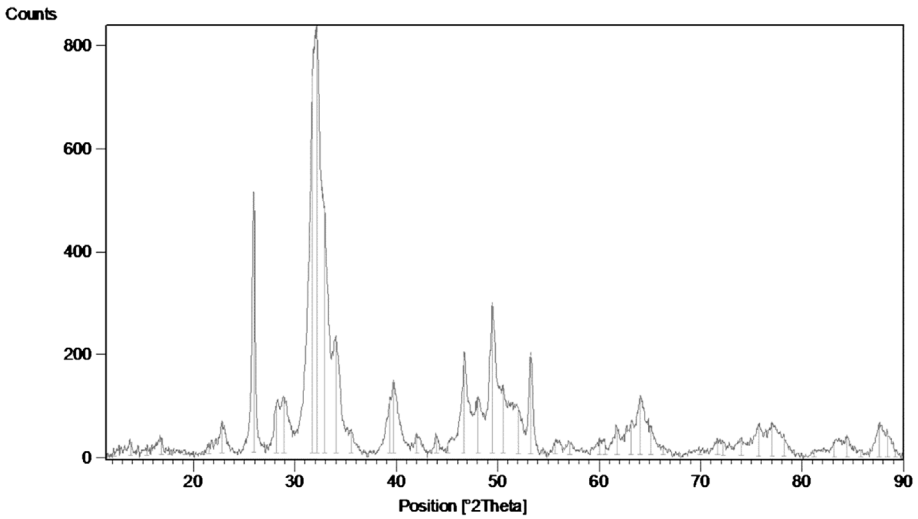

Figure 1 XRD pattern of HA powder (the reported bars indicate the JCPDS 09–432 phase)

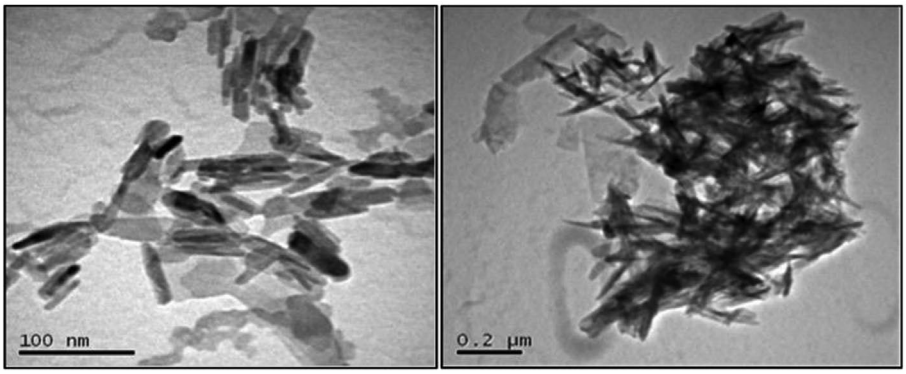

Figure 2 TEM images of HA powder

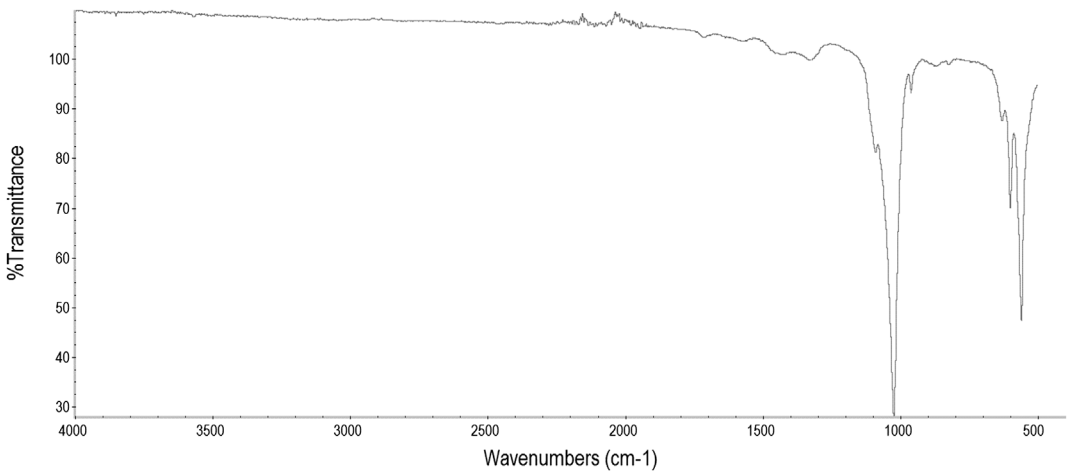

Figure 3 IR spectrum of HA powder

TEM micrographs of the synthesized HA powder are reported in Fig. 2, showing particles of acicular shape with an average length between 50 and 200 nm and an average diameter between 10 and 30 nm, with an average aspect ratio of about 6. The particles tend to form roughly spherical agglomerates of about 100 nm to decrease their high surface energy.

In Table 1, the powder SSA value is reported which is necessary to evaluate the content of silane coupling agent that was added to control the suspension stability. The powder showed a value of SSA of 117 $m^2\ g^{-1}$, indicating the high surface/volume ratio of the nanoparticles that could be estimated around $100 \times 10^{-6}\ m^{-1}$. As mentioned in paragraph 2.2, 7.9 g of silane coupling agent were then added to the HEMA/HA suspension.

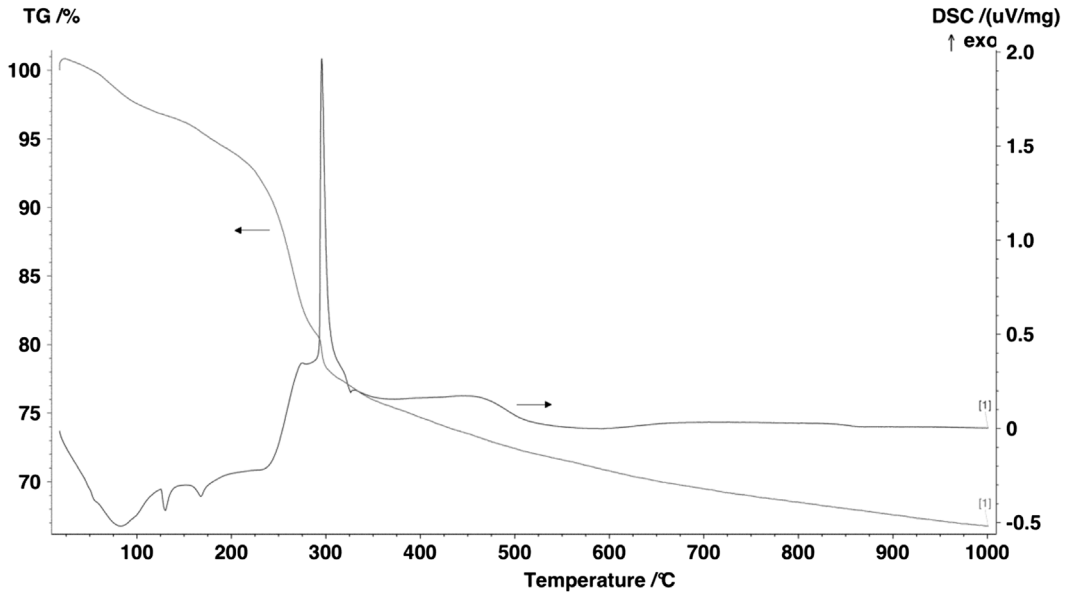

Figure 4 TG/DTA curves of HA powder

Table 3 Thermal and dynamic-mechanical properties (E': conservative modulus, tanδ$_{max}$: maximum value of loss factor)

Sample	T_g (°C) by DSC	E' elastic region 29 °C (GPa)	E' rubbery region 145 °C (MPa)	E' Mooney region 145 °C s=1.35	T_g (°C) by DMTA (tanδ$_{max}$)
Unfilled 1:2	66	2.27	1.4	1.4	98
1:2 HA	76	4.21	9.4	2.1	109
Unfilled 1:3	68	3.91	1.2	1.2	102
1:3 HA	83	3.09	10.0	1.9	103

Figure. 3 shows the IR spectra of the obtained powders. The formation of HA is indicated by the presence of an intense peak centered at around 1000–1100 cm^{-1}, since the phosphate bands v3 fall in the region 1092–1048 cm^{-1} (corresponding to triply degenerated anti-symmetric P–O stretching). Moreover, the v1 at 963 cm^{-1} (corresponding to non-degenerate symmetric P–O stretching), v4 at 603 and 571 cm^{-1} (corresponding to triply degenerated O–P–O bending)[32] are present. Finally, a weak broad band can be observed in the range between 3100 and 3600 cm^{-1} that corresponds to the presence of OH groups.[33] The small peak observed between 1200 and 1350 cm^{-1} could be due to the silane coupling agent as the Si-O-CH$_3$ vibrational state falls at 1207 cm^{-1} (Si-O bending).[34]

TG-DTA analysis (Fig. 4) performed on the same sample confirmed the absence of secondary calcium phosphate phases; the curves revealed the endothermic loss of water molecules at 100 °C and the exothermic crystallization of the amorphous HA phase at 280 °C associated with the elimination of some volatile components present as traces in initial reagents.[22] The exothermic weight loss at 300 °C might be due to combustion of the organic residue probably associated with the silane coupling agent. Finally, the weight loss observed in the range of 400–1000 °C is assumed as the gradual dehydroxylation in the HA powder. These results assure that, during the curing step (1 h at 60 °C with post cure at 100 °C for another hour) of the PMMA/HEMA/HA composites, the HA powder is stable and does not undergo any structural changes.

Nanocomposites characterization

The glass transition temperatures, evaluated by DSC analysis (Table 3), were significantly affected by the presence of HA, as a strong increase was observed in the nanocomposites in comparison with the respective unfilled matrix for both HA contents. This effect is attributed to a stiffening effect due to interactions between the polymer matrix and the filler in the interfacial region.[35]

DMTA results (Figs. 5 and 6) showed that the nanocomposites dynamic-mechanical properties, such as storage modulus, loss modulus and tanδ, were affected by the HA content. This is an expected behavior due to the addition of rigid fillers to polymer matrix that contrasts the movement of the polymer chains leading to a damping decrement and a shift of T_g values to higher temperatures.[36]

The glass transition temperature (T_g) at maximum value of loss factor, tanδ, and storage modulus E′ at the elastic region and rubbery region obtained by DMTA are also reported in Table 3. In the low temperature region (below T_g), the storage modulus does not follow a systematic trend with composition showing the highest value in the case of 1:2 HA sample and, surprisingly, a higher value for unfilled 1:3 sample with respect to the corresponding filled one (1:3 HA). On the contrary, a significant increase in storage modulus E′ in the rubbery region was observed in both nanocomposites, as they presented a value of E′ almost 10 times

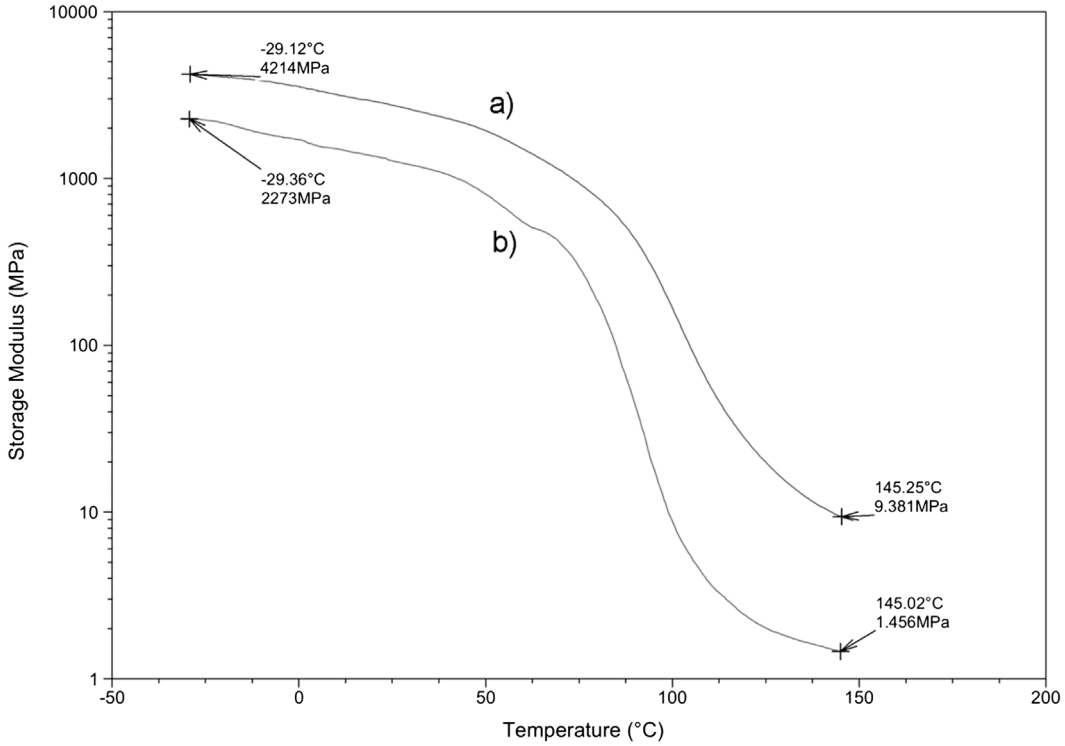

Figure 5 Conservative modulus (E') trace of *a* 1:2 HA and *b* unfilled 1:2 (chosen as representative)

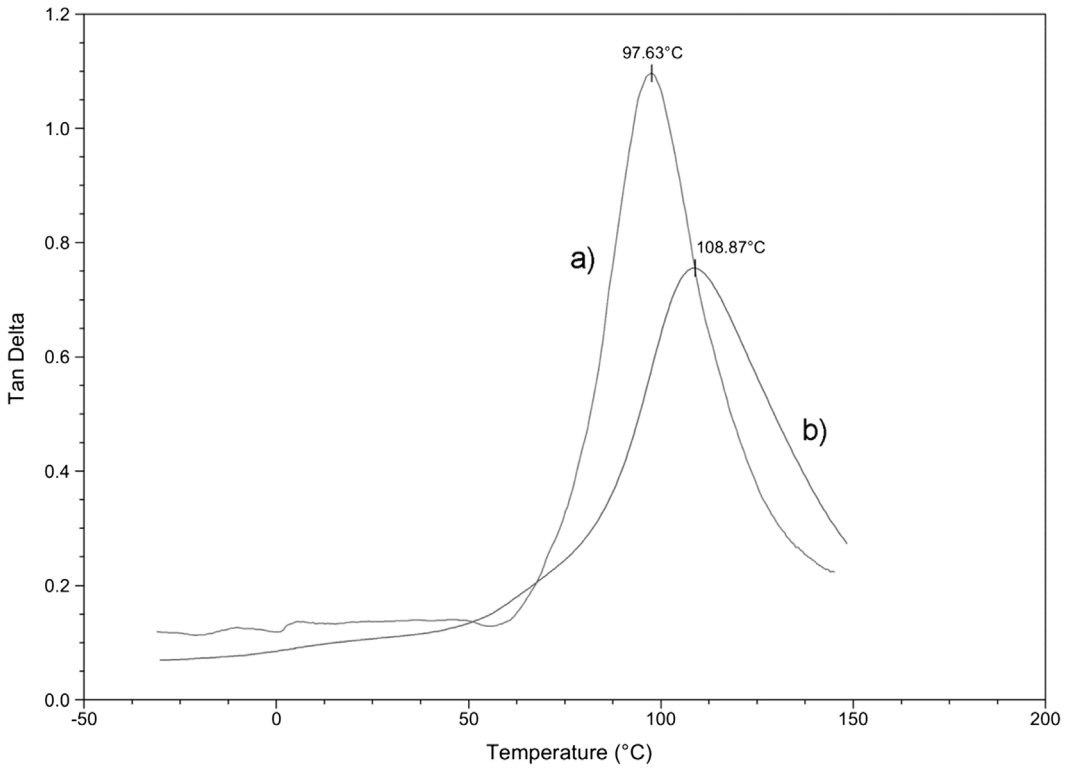

Figure 6 Loss factor (tanδ) trace of *a* 1:2 HA and *b* unfilled 1:2 (chosen as representative)

higher than the respective unfilled samples. As expected, lower values of tanδ (loss factor) in the nanocomposites were also observed even at high temperature indicating a lower damping in the nanocomposites due to the interaction between the filler and the polymer matrix.

In order to compare the experimental results with data predicted by the well-known models for composite materials, Mooney's empirical equation for non-spherical particles[37] was applied to study the dependence of the elastic modulus of filled polymers on the nanoparticles content.

Table 4 Flexural and compression modulus as experimentally obtained and calculated by Equation (2)

	E_c experimental (MPa)	E_c Mooney (MPa)	E_f experimental (MPa)	E_f Mooney (MPa)
Unfilled 1:3	226 ± 87	226	347 ± 122	347
1:3 HA	256 ± 56	361	662 ± 197	552

Table 5 Experimental and calculated composite strength (σ)

	σ experimental (MPa)	σ Nielsen (MPa)	σ Pukanszky* (MPa)
Unfilled 1:3	15 ± 5.33	15	15
1:3 HA	8.2 ± 1.1	13.5	15.1

*calculated assuming a good adhesion: $B = 3.5$.

Table 6 Water sorption values

Sample	W_{sp} (μg·mm^{-3})
Unfilled 1:2	297
1:2 HA	290
Unfilled 1:3	369
1:3 HA	291

$$\frac{E_c}{E_m} = \exp\left(\frac{2.5V_p + 0.407(p-1)^{1.508}V_p}{1 - sV_p}\right) \quad (2)$$

where *Ec* and *Em* are the Young's modulus of composite and matrix, *Vp* is the particle volume fraction, *p* is the aspect ratio of the filer, *s* is a crowding factor for the ratio of the apparent volume occupied by the particle to its own true volume. The value of *s* lies between 1.35 and 1.91, where the minimum value of s comes from the least dense packing factor, which is the sphere packaging factor ($s = 3\sqrt{2}/\pi \cong 1.35$), while the maximum value of *s* comes from the densest cubic factor ($s = \frac{6}{\pi} \cong 1.91$)

As shown in Table 3, the values of the obtained storage modulus, in the rubbery region, are higher than the data predicted by Mooney's equation and the crowding factor had no significant effect due to the very low filler content.

The high increment of the storage modulus obtained in the nanocomposites has been also observed in previous studies such as;[36] considering that in the rubbery region, the modulus value is principally governed by the cross-linking density, an increase in the latter could be attributed to the presence of

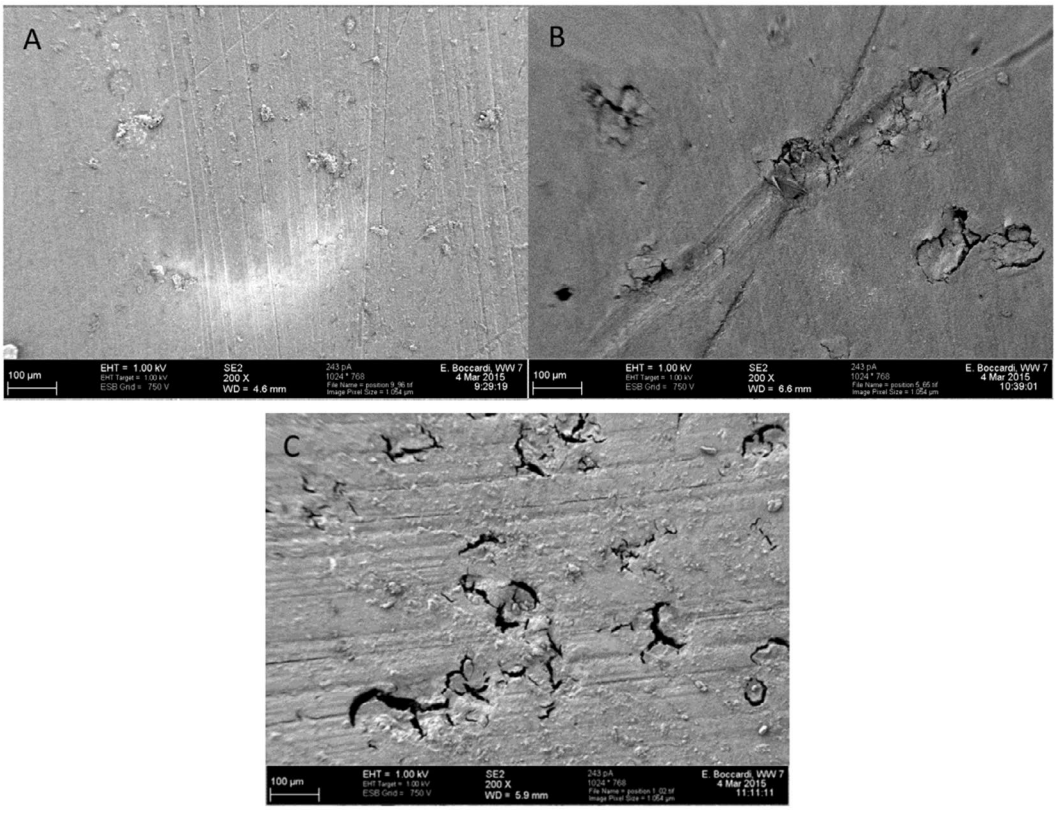

Figure 7 Surface morphology of the samples: (A) unfilled, (B) 1:2 HA, (C) 1:3 HA

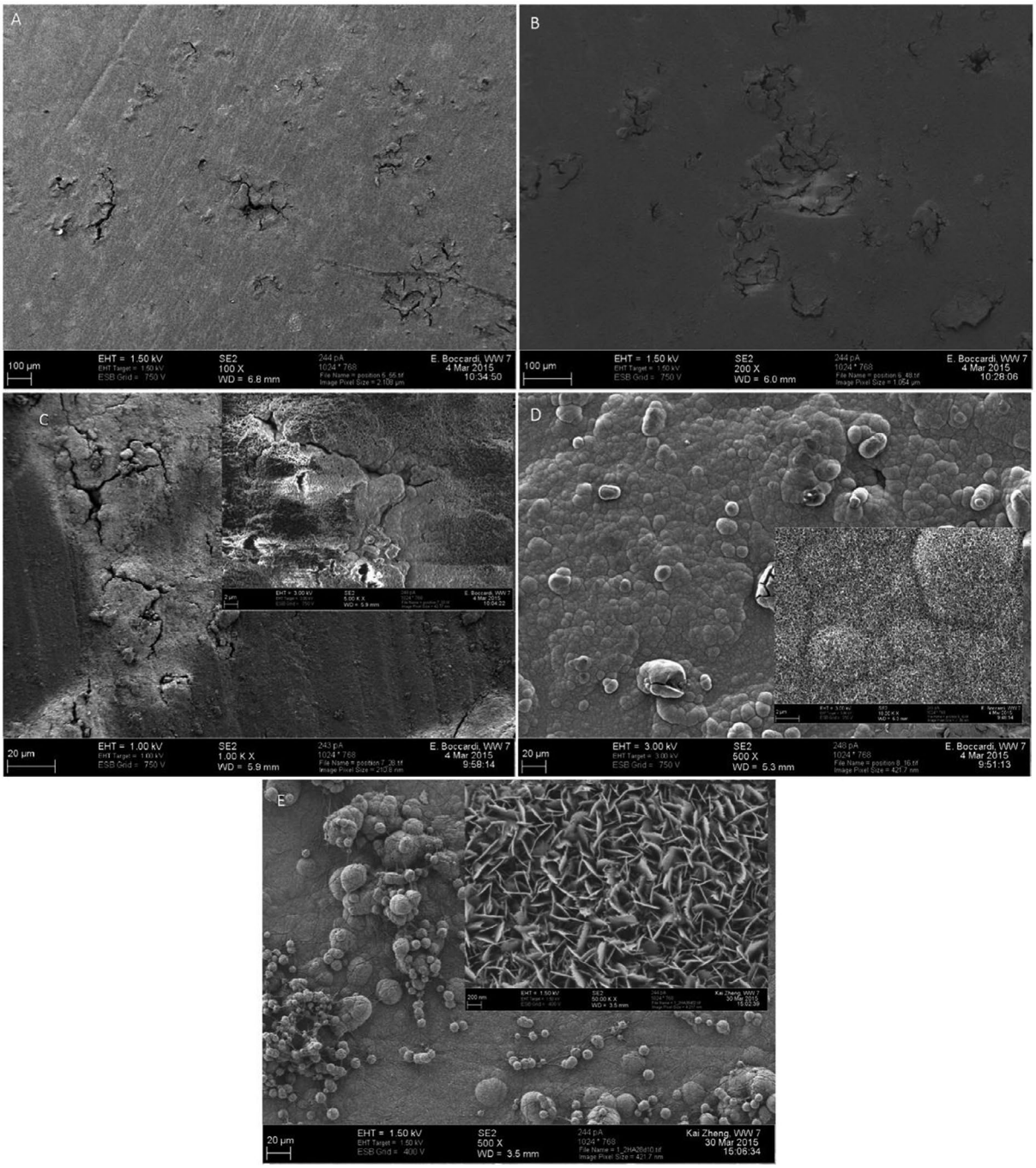

Figure 8 SEM images of 1:2 HA after SBF treatment: (A) untreated; (B) 1 h; (C) 24 h; (D) 7 d; (E) 28 d

the *in situ* generated HA, therefore, the HA nanoparticles could act not only as rigid reinforcing filler but also as cross-linking points.

In Table 4, the results of the flexural and compression tests on 1:3 filled and unfilled samples are reported. The flexural test showed an increment of the flexural modulus for nanocomposite by 52% that is an expected result since in the composites the deformations are strongly obstructed by the nanofiller. However, the nanocomposite presented a brittle fracture before the yield point was reached and a lower value of the flexural strength, probably due to the presence of certain agglomeration that acts as stress concentrations. The compression tests gave a value of compression modulus of the nanocomposite greater than that of the unfilled of almost 12%.

The values of the E_f and E_c were also compared with data predicted using Equation (2). As it can be seen in Table 4, for the flexural test, the increment obtained is greater than the increment predicted by the Mooney's equation while in the case of the compression test, the theoretic and the experimental results are very close considering the experimental error, probably because the effect of the filler is more evident in case of flexural deformation.

For the flexural strength, two different empirical equations were applied, considering the cases of good and poor interfacial adhesion.

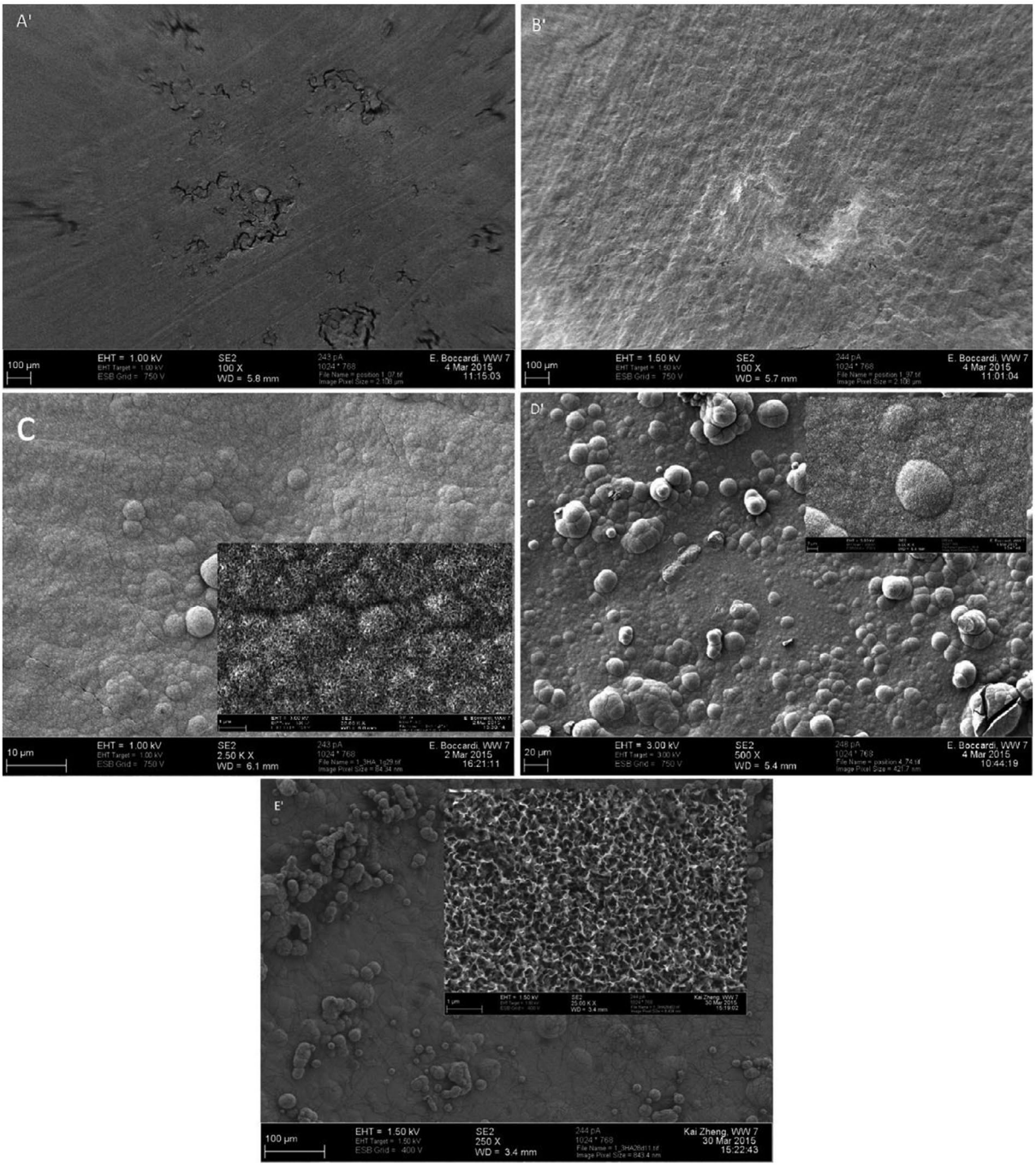

Figure 9 SEM images of 1:3 HA after SBF treatment: (A) untreated; (B) 1 h; (C) 24 h; (D) 7 d; (E) 28 d

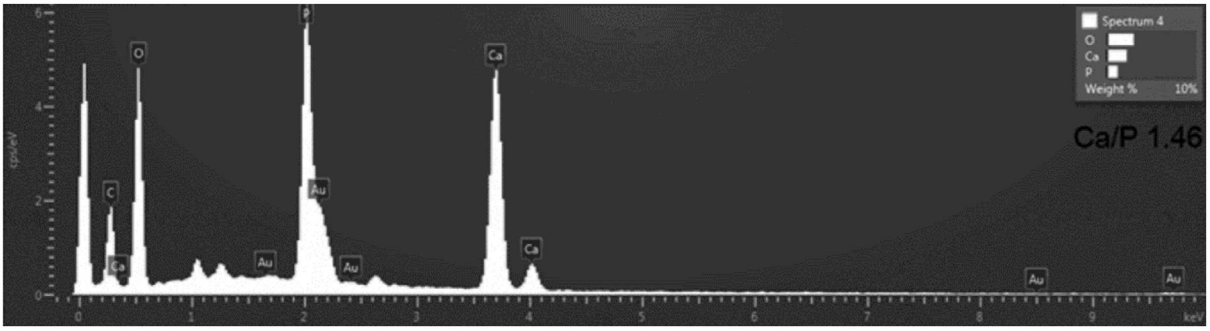

Figure 10 EDS spectrum of 1:2 HA apatite layer, sample (D)

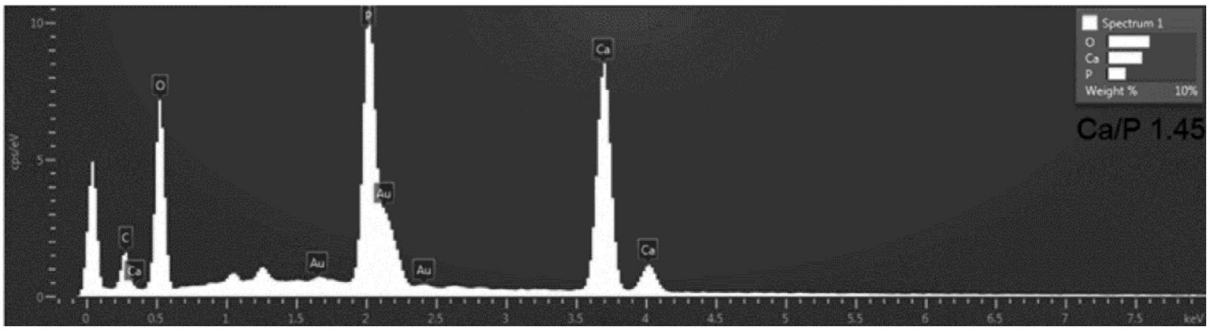

Figure 11 EDS spectrum of 1:3 HA apatite layer, sample (D)

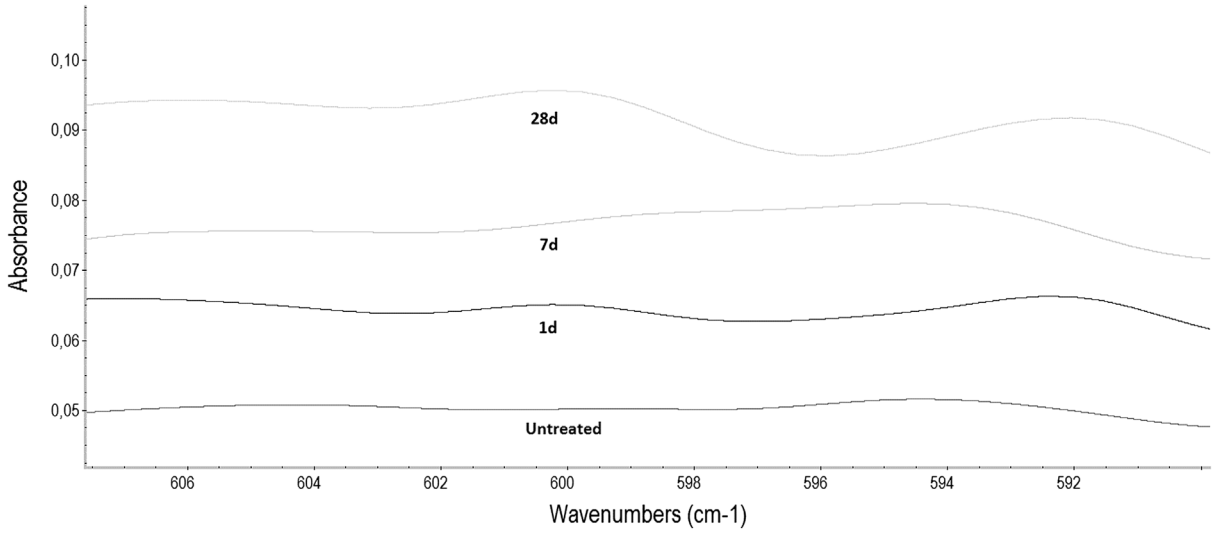

Figure 12 FT-IR spectra of 1:2 HA after SBF treatment

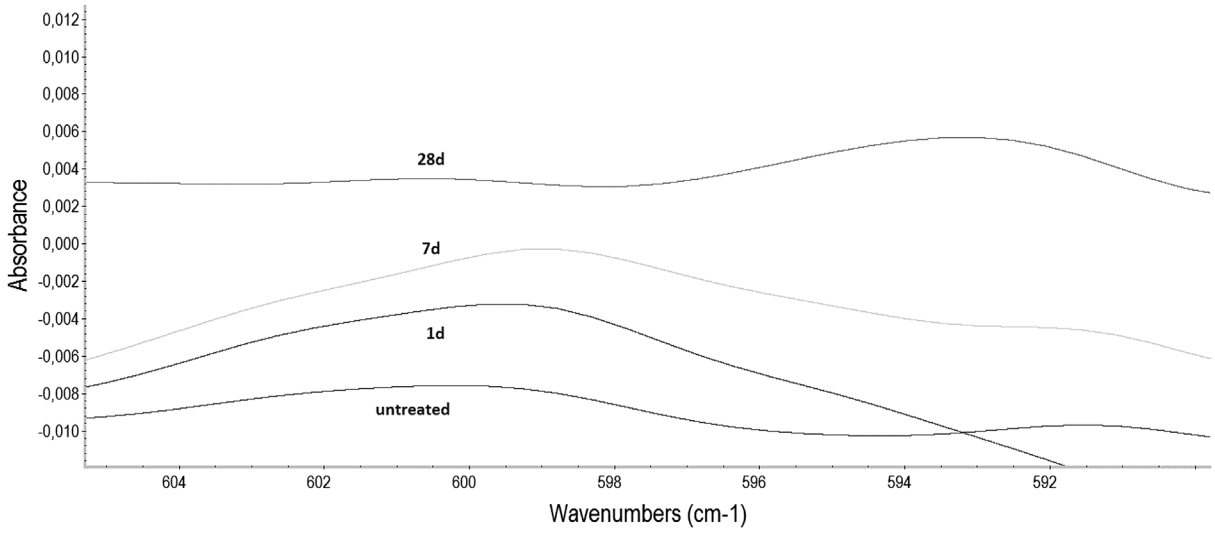

Figure 13 FT-IR spectra of 1:3 HA after SBF treatment

The Nielsen's equation for poorly bonded particles[37] is shown below:

$$\sigma_c = \sigma_m\left(1 - Vp^{\frac{2}{3}}\right)Q \qquad (3)$$

where σ_c and σ_m are the strength of the composite and the matrix, *Vp* is the particles volume fraction and the parameter *Q* accounts for weaknesses in the structure caused by the discontinuities in stress transfer and generation of stress concentration at the particle/polymer interface. When there is no stress

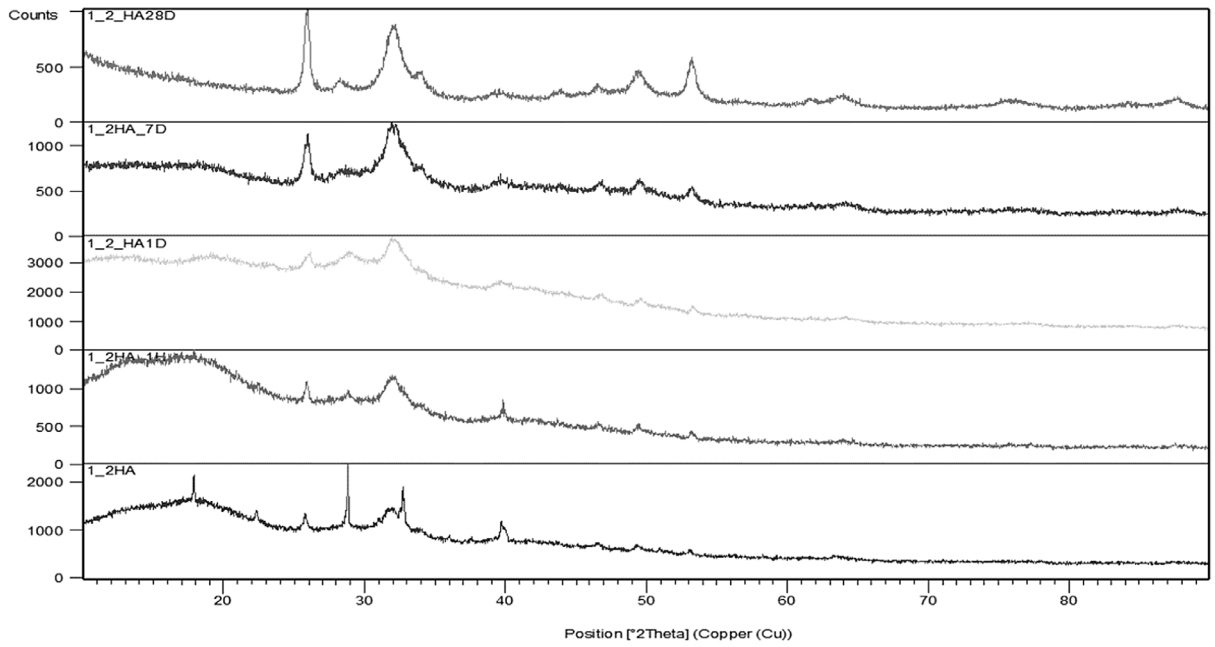

Figure 14 XRD patterns of 1:2 HA after SBF treatment (from the bottom: untreated and after 1 h, 24 h, 7 d, 28 d)

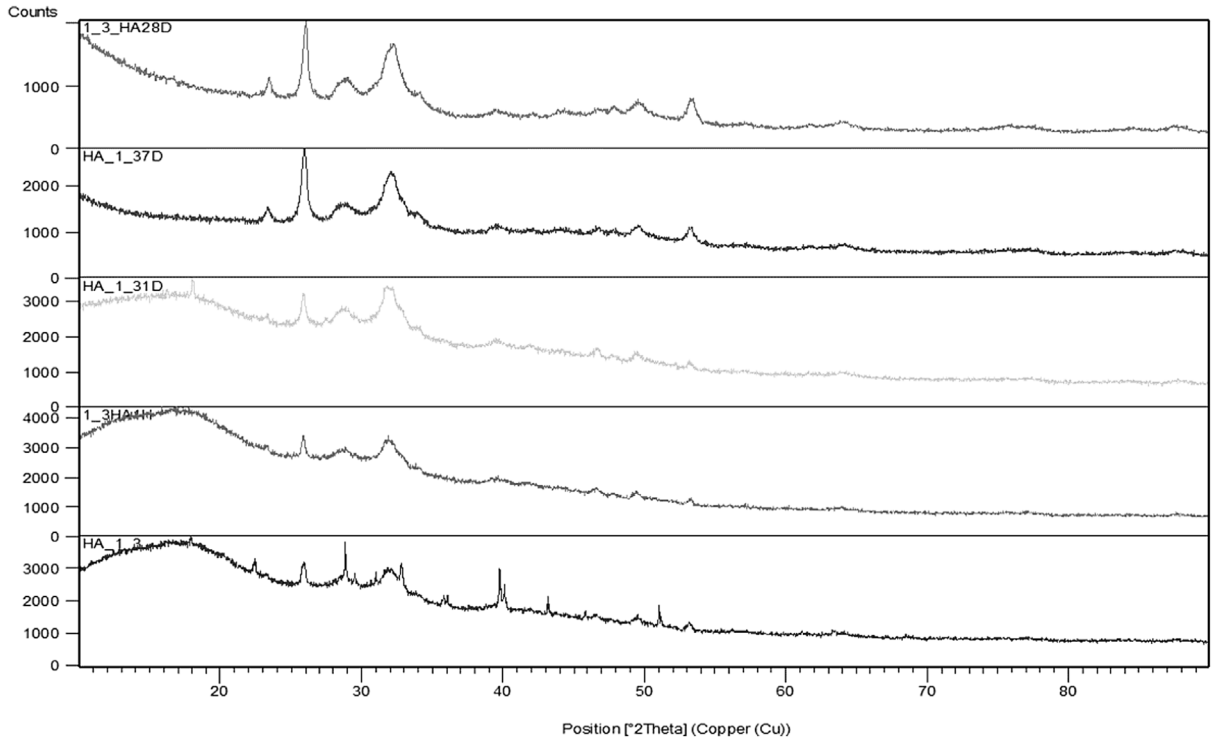

Figure 15 XRD patterns of 1:3 HA after SBF treatment (from the bottom: untreated and after 1 h, 24 h, 7 d, 28 d)

concentration, the value of Q is equal to 1, Q was considered equal to one (case of no stress concentrations) to determine the value of the predicted flexural strength. To determine the stress concentrations in the nanocomposite, the value of Q was determined using the experimental value of σ_c

In case of strong particle-matrix interfacial bonding, Pukanszky's equation[37] can be applied:

$$\sigma_c = \left[\frac{1 - Vp}{1 + 2.5Vp}\sigma_m\right] \exp(BVp) \quad (4)$$

where B is an empirical constant, which depends on the surface area of particles, particle density, and interfacial bonding energy, B is equal to zero in case of poor interfacial bonding that means that the particles do not carry any load while for good adhesion assumes values around 3.5. The obtained results are listed in Table 5.

The Table clearly shows that using the Nielsen's equation for poorly bonded particles ($Q = 1$), the strength of the composite decreases by 10% with respect of the unfilled sample;

instead in case of good adhesion, the empirical equation proposed by Pukanszky gives an increment of the flexural strength of 0.7%.

Analyzing the predicted data in comparison with the experimental data, because the strength of the filled polymer decreases by 45%, it can be concluded that the bulk samples are affected by the presence of stress concentration and *Q* assumes value of 0.61.

Finally, the values of the sample water sorption are listed in Table 6. The data showed that the effect of HA is more remarkable in the case of 1:3 HA as it reduces the water sorption by 21%. This effect could be explained considering the nanoparticles acting as crosslinking points, therefore the cross-linking density of the nanocomposite is higher than the unfilled leading to a smaller water sorption capacity. The effect on the water sorption, however, is mainly determined by the presence of the hydroxyl groups in HEMA, as the samples with PMMA/HEMA ratio 1:3 present a higher value of water sorption.

The SEM micrograph in Fig. 7 shows the presence of cracks on the surface of the nanocomposite samples (1:2 and 1:3 HA) with an average length of about 100 μm. This was probably due to the presence air bubbles that remained trapped in the suspensions during reticulation. These cracks are absent in the unfilled sample and this should be the explanation of the high stress concentrations observed on the nanocomposites in the flexural test.

Concerning bioactivity analysis, SEM micrographs (Figs. 8 and 9) show that after one hour of immersion in SBF, there is no trace of a HA deposit on the surface of both unfilled (here not reported) and composite samples. After one day of immersion, a layer of deposit starts forming exhibiting a typical apatite morphology on the surface of both composite samples 1:2 and 1:3 HA. The short time needed for the apatite layer deposition is related to a high degree of bioactivity, and it could be due to the high specific surface area of the nanorods of hydroxyapatite, as this particular shape presents better adsorption (even HA present in human tooth and bone exhibits the form of nano-polycrystalline hexagonal nanorods[33]) and the presence of the OH groups of HEMA which confers more absorbance to the material.

After seven days of immersion, both the composite samples were almost completely covered by the apatite layer: no trace of a deposit was observed in the unfilled sample (here not reported), while a complete coverage of the surface of the nanocomposites was observed after 28 days of treatment.

EDS analysis (Figs. 10 and 11) of the formed layer allowed its identification as hydroxyapatite, since it shows that it consist of Ca and P with atomic ratio in the range between 1.43 and 1.5 that is close to the Ca/P ratio of natural hydroxyapatite (1.6).

FT-IR spectroscopy (Figs. 12 and 13) shows a small shift of two peaks at around 604 and 592 cm^{-1} in the nanocomposites, which correspond to the P–O vibration of PO_4^{3-} in hydroxyapatite; the shift is more evident in samples treated for 28 days in SBF, while a small signal is also present in the untreated samples due to the presence of HA nanoparticles.

The presence of HA crystallized on the sample surface was also observed in the XRD patterns (Figs. 14 and 15). In the untreated composites, small peaks, related to the HA nanoparticles present in the polymer matrix, are observed with large percentage of amorphous phase; increasing soaking time in SBF, independently on the PMMA/HEMA ratio, an increase of the amount of crystalline hydroxyapatite phase, that become predominant after 28 days of treatment, can be observed.

Conclusions

PMMA/PHEMA polymer blends with hydroxyapatite as nanofiller were successfully prepared through the 'reactive suspension method'. Nanosized hydroxyapatite was *in situ* synthesized by co-precipitation process in the presence of hydroxyethyl methacrylate as suspending medium reactive toward the subsequent polymerization. FT-IR and XRD analysis confirmed the formation of hydroxyapatite and TEM microscopy revealed that HA nanorods with an aspect ratio value between 5 and 7 were obtained.

DSC analysis showed a significant increase in glass transition temperature in the nanocomposites with respect to the unfilled polymer blends. Dynamic mechanical analysis showed a significant increment in the nanocomposite of the storage modulus measured in the rubbery region (above glass transition temperature) unpredicted by the usual predictive equations which can be attributed to the presence of cross-linking points due to the *in situ* generated particles. An increment of the elastic modulus was also observed at room temperature in compression and three-point bending tests. The presence of hydroxyapatite in the polymer blends resulted in an important decrease in the water sorption values. Excellent results in terms of bioactivity were also obtained in the case of composites containing *in situ* prepared hydroxyapatite.

Acknowledgments

The authors would like to acknowledge Kai Zheng and Dirk Dippold for their contribution in the characterization of the bioactivity of the samples, for the SEM and FT-IR analysis.

Disclosure statement

No potential conflict of interest was reported by the authors.

ORCID

Federica Bondioli http://orcid.org/0000-0002-4507-3831
Sergio Bortolini http://orcid.org/0000-0003-3700-4286
Massimo Messori http://orcid.org/0000-0003-3598-4241

References

1. L. Cheng, X. Zhou, H. Zhong, X. Deng, Q. Cai and X. Yang: 'NaF-loaded core-shell PAN-PMMA nanofibers as reinforcements for Bis-GMA/TEGDMA restorative resins', *Mater. Sci. Eng. C Mater. Biol. Appl.*, 2014, **34**, 262–269.
2. X. Y. Zhang, X. J. Zhang, Z. L. Huang, B. S. Zhu and R. R. Chen: 'Hybrid effects of zirconia nanoparticles with aluminum borate whiskers on mechanical properties of denture base resin PMMA', *Dent. Mater. J.*, 2014, **33**, 141–146.
3. N. Kojima, M. Yamada, A. Paranjpe, N. Tsukimura, K. Kubo, A. Jewett and T. Ogawa: 'Restored viability and function of dental pulp cells on polymethylmethacrylate (PMMA)-based dental resin supplemented with N-acetyl cysteine (NAC)', *Dent. Mater.*, 2008, **24**, 1686–1693.

4. W. Yu, X. Wang, Q. Tang, M. Guo and J. Zhao: 'Reinforcement of denture base PMMA with ZrO(2) nanotubes', *J. Mech. Behav. Biomed. Mater.*, 2014, **32**, 192–197.
5. I. N. Safi: 'Evaluation the effect of nano-fillers (TiO2, Al2O3, SiO2) addition on glass transition temperature, e-moudulus and coefficient of thermal expansion of acrylic denture base material', *J. Baghdad Coll. Dent.*, 2014, **26**, 37–41.
6. J. C. Zhang, J. Liao, A. C. Mo, Y. B. Li, J. D. Li and X. J. Wang: 'Characterization and human gingival fibroblasts biocompatibility of hydroxyapatite/PMMA nanocomposites for provisional dental implant restoration', *Appl. Surf. Sci.*, 2008, **255**, 328–330.
7. M. Supova, G. S. Martynkova and K. Barabaszova: 'Effect of Nanofillers Dispersion in Polymer Matrices: A Review', *Sci. Adv. Mater.*, 2011, **3**, 1–25.
8. F. Tan, M. Naciri, D. Dowling and M. Al-Rubeai: '*In vitro* and *in vivo* bioactivity of CoBlast hydroxyapatite coating and the effect of impaction on its osteoconductivity', *Biotechnol. Adv.*, 2012, **30**, 352–362.
9. P. Wutticharoenmongkol, P. Pavasant and P. Supaphol: 'Osteoblastic phenotype expression of MC3T3-E1 cultured on electrospun polycaprolactone fiber mats filled with hydroxyapatite nanoparticles', *Biomacromolecules*, 2007, **8**, 2602–2610.
10. A. P. Marques and R. L. Reis: 'Hydroxyapatite reinforcement of different starch-based polymers affects osteoblast-like cells adhesion/spreading and proliferation', *Mater. Sci. Eng. C*, 2005, **25**, 215–229.
11. L. Shor, S. Guceri, X. Wen, M. Gandhi and W. Sun: 'Fabrication of three-dimensional polycaprolactone/hydroxyapatite tissue scaffolds and osteoblast-scaffold interactions *in vitro*', *Biomaterials*, 2007, **28**, 5291–5297.
12. F. Causa, P. A. Netti, L. Ambrosio, G. Ciapetti, N. Baldini, S. Pagani, et al: 'Poly-epsilon-caprolactone/hydroxyapatite composites for bone regeneration: *in vitro* characterization and human osteoblast response', *J. Biomed. Mater. Res. A.*, 2006, **76**, 151–162.
13. V. Guarino, F. Causa, P. A. Netti, G. Ciapetti, S. Pagani, D. Martini, N. Baldini and L. Ambrosio: 'The role of hydroxyapatite as solid signal on performance of PCL porous scaffolds for bone tissue regeneration', *J. Biomed. Mater. Res. B Appl. Biomater.*, 2008, **86**, 548–557.
14. S. J. Heo, S. E. Kim, Y. T. Hyun, D. H. Kim, H. M. Lee, Y. M. Hwang, S. A. Park and J. W. Shin: '*In vitro* evaluation of poly epsilon-caprolactone/hydroxyapatite composite as scaffolds for bone tissue engineering with human bone marrow stromal cells', *Key Eng, Mat.*, 2007, **342–343**, 369–372.
15. D. Verma, K. Katti and D. Katti: 'Bioactivity in *in situ* hydroxyapatite-polycaprolactone composites', *J. Biomed. Mater. Res. A.*, 2006, **78**, 772–780.
16. P. Fabbri, F. Bondioli, M. Messori, C. Bartoli, D. Dinucci and F. Chiellini: 'Porous scaffolds of polycaprolactone reinforced with *in situ* generated hydroxyapatite for bone tissue engineering', *J. Mater. Sci. Mater. Med.*, 2010, **21**, 343–351.
17. M. Catauro, M. G. Raucci, F. De Gaetano and A. Marotta: 'Sol-gel synthesis, characterization and bioactivity of polycaprolactone/SiO2 hybrid material', *J. Mater. Sci.*, 2003, **38**, 3097–3102.
18. M. Catauro, M. G. Raucci, F. de Gaetano, A. Buri, A. Marotta and L. Ambrosio: 'Sol-gel synthesis, structure and bioactivity of polycaprolactone/CaO. SiO2 hybrid material', *J. Mater. Sci. Mater. Med.*, 2004, **15**, 991–995.
19. D. Hakimimehr, D. M. Liu and T. Troczynski: 'In-situ preparation of poly(propylene fumarate)–hydroxyapatite composite', *Biomaterials*, 2005, **26**, 7297–7303.
20. S. Z. C. Liou, S. Y. Chen and D. M. Liu: 'Phase development and structural characterization of calcium phosphate ceramics-polyacrylic acid nanocomposites at room temperature in water-methanol mixtures', *J. Mater. Sci.-Mater. M.*, 2004, **15**, 1261–1266.
21. F. Bakan, O. Lacin and H. Sarac: 'A novel low temperature sol-gel synthesis process for thermally stable nano crystalline hydroxyapatite', *Powder Technol.*, 2013, **233**, 295–302.
22. A. Y. Fadeev, R. Helmy and S. Marcinko: 'Self-assembled monolayers of organosilicon hydrides supported on titanium, zirconium, and hafnium dioxides'. *Langmuir*, 2002, **18**, 7521–7529.
23. ISO IS: 'Polymer-based restorative materials', 4th edn, 2009, 4049 Dentistry.
24. ISO IS: 'Determination of compressive properties', 2002, 04 Pastics.
25. T. Kokubo and H. Takadama: 'How useful is SBF in predicting *in vivo* bone bioactivity?' *Biomaterials.*, 2006, **27**, 2907–2915.
26. F. W. Liu, X. Z. Jiang, Q. H. Zhang and M. F. Zhu: 'Strong and bioactive dental resin composite containing poly(Bis-GMA) grafted hydroxyapatite whiskers and silica nanoparticles', *Compos. Sci. Technol.*, 2014, **101**, 86–93.
27. R. Kamalian, A. Yazdanpanah, F. Moztarzadeh, R. Ravarian, Z. Moztarzadeh, M. Tahmasbi and M. Mozafari: 'Synthesis and characterization of bioactive glass/forsterite nanocomposites for bone and dental implants', *Ceram.-Silikaty*, 2012, **56**, 331–340.
28. S. M. Abo-Naf, E. S. M. Khalil, E. S. M. El-Sayed, H. A. Zayed and R. A. Youness: 'In vitro bioactivity evaluation, mechanical properties and microstructural characterization of Na2O-CaO-B2O3-P2O5 glasses'. *Spectrochim. Acta A.*, 2015, **144**, 88–98.
29. J. Loof, F. Svahn, T. Jarmar, H. Engqvist and C. H. Pameijer: 'A comparative study of the bioactivity of three materials for dental applications', *Dent. Mater.*, 2008, **24**, 653–659.
30. Q. Chen, I. Thompson and A. R. Boccaccini: 'Bioglass-derived glass-ceramic scaffolds for bone tissue engineering', *Biomaterials*, 2006, **17**, 2414–25.
31. D. N. Ungureanu, N. Angelescu, R.M. Ion, E.V. Stoian and C. Z. Rizescu: 'Synthesis and Characterization of Hydroxyapatite Nanopowders by Chemical Precipitation', in '*Recent Researches in Communications, Automation, Signal Processing, Nanotechnology, Astronomy and Nuclear Physics*', (eds. Z. Bojkovic, J. Kacprzyk, N. Mastorakis, V. Mladenov, R. Revetria, L. A. Zadeh, & A. Zemliak), 296–301; 2011, WSEAS Press, Cambridge, ISBN: 978-960-474-276-9.
32. B. C. E. Idrissia, K. Yamnib, A. Yacoubia and A. Massita: 'A novel method to synthesize nanocrystalline hydroxyapatite: Characterization with X-ray diffraction and infrared spectroscopy', *J. Appl. Chem.*, 2014, **7**, 107–112.
33. S. K. Padmanabhan, A. Balakrishnan, M. C. Chu, Y. J. Lee, T. N. Kim and S. J. Cho: 'Sol-gel synthesis and characterization of hydroxyapatite nanorods', *Particuology*, 2009, **7**, 466–470.
34. N. A. Rangel-Vazquez and T. Leal-Garcia: 'Spectroscopy Analysis of Chemical Modification of Cellulose Fibers', *J. Mex. Chem. Soc.*, 2010, **54**, 192–197.
35. R. Qiao, H. Deng, K. W. Putz and L. C. Brinson: 'Effect of particle agglomeration and interphase on the glass transition temperature of polymer nanocomposites', *J. Polym. Sci. Pol. Phys.*, 2011, **49**, 740–748.
36. D. Morselli, F. Bondioli, M. Sangermano and M. Messori: 'Photo-cured epoxy networks reinforced with TiO2 *in situ* generated by means of non-hydrolytic sol-gel process', *Polymer*, 2012, **53**, 283–290.
37. S. Y. Fu, X. Q. Feng, B. Lauke and Y. W. Mai: 'Effects of particle size, particle/matrix interface adhesion and particle loading on mechanical properties of particulate-polymer composites', *Compos. Part B-Eng.*, 2008, **39**, 933–961.